An automatic docking method for large-scale sections based on real-time pose measuring and assembly deviation control*

QIAO Zhifeng[1,2]**, FU Kang[1,2], and LIU Zhenzhong[1,2]

1. *Tianjin Key Laboratory for Advanced Mechatronic System Design and Intelligent Control, School of Mechanical Engineering, Tianjin University of Technology, Tianjin 300384, China*

2. *National Demonstration Center for Experimental Mechanical and Electrical Engineering Education, Tianjin University of Technology, Tianjin 300384, China*

Aiming at the problem of poor accuracy consistency of large sections' docking assembly, an automatic docking method using multiple laser trackers to measure the position and posture of the docking sections in real time was proposed. In the solution of the pose of the docking section, real-time pose measurement of the docking section was realized by establishing a global coordinate system and a coordinate fusion method of three or more laser trackers. In the automatic control of the docking process, the real-time communication protocol and the circular negative feedback control strategy of measurement-adjustment-re-measurement are adopted, and the fully-automated docking of large sections is realized. Finally, an experimental verification system was set up, and the docking of the large-scale section reduction models was realized under the requirements of docking accuracy, and the effectiveness of the automatic docking scheme was successfully verified.

For the adjustment and docking of some large-scale sections in the aerospace field, designing unique positioning and docking process equipment is necessary. Traditional positioning and docking equipment generally adopts a purely mechanical manual operation scheme, which requires multiple people to coordinate the operation to complete the positioning and docking. The problem of poor consistency of the docking assembly accuracy generally exists[1-4]. With the development of industrial control technology, especially the extensive application of multi-axis movement control technology and fieldbus communication technology, large-scale digital positioning and docking equipment with comprehensive range operations, high degree of freedom (DOF) for adjustment, and high real-time centralized control requirement have become a reality[2,5-7]. Meanwhile, large-scale docking sections' position and pose measurement technology has also been more maturely applied. The technology of using laser trackers, binocular photography, and indoor global positioning system (GPS) technology to run pose measurements of large-scale sections have also been involved in the field of aerospace[3,8-10], which makes the realization of real-time pose adjustment and docking assembly of large-scale product sections by using real-time measurement feedback and multi-axis movement control possible.

In the real-time and accurate measurement of the pose of large-scale sections, for the binocular photography solution, there is a limited range of photography, low real-time measurement feedback, and the inconvenience of changing the measurement range because the camera needs to be fixed[10,11]. Ref.[9] proposed a binocular photography scheme and calibration method using a Telecentric lens, which is expected to further improve the measurement accuracy of the binocular photography system. However, the increase in the measurement distance still dramatically impacts the measurement system's accuracy, making it challenging to use this technology in the pose measurement of large sections (5 m and above) in the aerospace field. Although the binocular photography positioning technology has the advantages of a wide measurement range and multiple targets that can be measured simultaneously, its measurement accuracy can only reach 0.25 mm in a 40 m working area.

Ref.[12] proposed an indoor positioning scheme that forwards GPS signals indoors to achieve low hardware requirements, which can achieve high horizontal positioning accuracy. Still, it is challenging to meet the criteria that the measurement accuracy should be within 0.1 mm of all directions in three-dimensional space in real-time automatic docking of large-scale docking sections[13,14], and because IGPS is limited by its measurement principle, multiple transmitters need to be placed in the measurement environment to achieve high accuracy, but its accuracy is not linear in number and will not increase after a certain number of transmitters in the environment. It is possible to measure the six-dimensional data of a single section by installing pose-measuring devices such as gyroscopes on the section. Still, large-scale docking section products often cannot be simply regarded as rigid objects. The posing data calculated after a single-point measurement often deviates significantly from the actual pose[15-19]. The measurement accuracy of the laser tracker solution can be within 0.01 mm, but a single laser tracker can only track one target point in real-time. When only a single laser tracker is used, a change of station is unavoidable, and this introduces more errors.

In the aerospace industry, it is particularly important to obtain the precise position of large parts and to monitor and adjust them in real-time during the entire assembly process[20]. So this paper proposes a method of real-time full-closed-loop measurement of the pose of a large section by using three or more laser tracking and real-time adjustment and docking of the pose of large sections by using a multi-axis motion controller. This method has a high accuracy for the measurements in all directions of three-dimensional space, addressing the limitations of GPS accuracy, limited range in binocular photography schemes, and errors introduced by using a single laser rangefinder that requires frequent repositioning.

As shown in Fig.1, the section products that need to be positioned and docked in aerospace are generally horizontal cylindrical. The design principle of the positioner is as simple as possible and easy to operate and control in a single movement direction. A single positioner can move along the direction of the product's *X*-axis, vertical *Z*-axis direction, and *Y*-axis direction determined by the right-hand rule according to the *X*-axis and *Z*-axis directions and the *Y*-direction of the product's rotation about its axis. Two positioners will form a group, and the pose adjustment of a typical section will be completed through cooperative work. There is no rigid connection mechanism such as a hinge between the tube section and the positioner to fix the positional relationship between the positioner and the tube section to facilitate the lifting and installation of large-scale docking sections. The product is lifted by the designed lifting point and placed directly on the positioner bearing bracket to complete the installation of a single section.
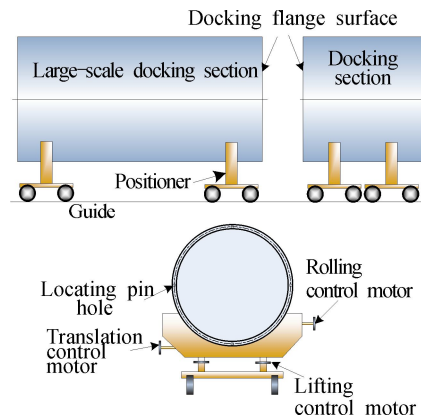

Fig.1 Positioning device diagram

The pose measurement of the assembly and docking process of large parts involves several coordinate systems: global coordinate system, laser tracker measurement coordinate system, fixed part coordinate system, and movable part coordinate system. In order to realize the coordinate unification of the measurement process, it is necessary to determine the conversion relationship between each coordinate system.

To complete the conversion of different coordinate systems, it is necessary to install a set of tracking target mirrors on the plant and docking parts and measure their coordinates on different objects using a laser tracker.

Fig.2 is a simplified view of the working environment of the plant. There are a number of global target points on the vertical beams in the plant called A_1, A_2, $A_3...A_n$, B_1, B_2, $B_3...B_n$, C_1, C_2, $C_3...C_n$. These global target points are precisely calibrated before measurement, which meet the line of points on the same vertical beam perpendicular to the geodetic reference system, the line of points on different vertical beams of the same name parallel to the global reference system, and their spacing has been in the measurement process to select any point as the origin of the global coordinate system position and establish the global coordinate system O_W-$X_WY_WZ_W$.
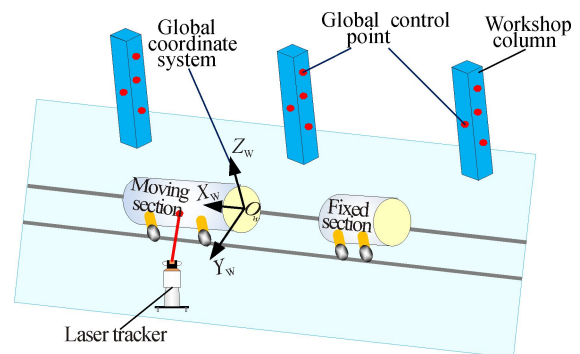

Fig.2 Establishment of a global coordinate system

The docking section comprises a fixed section and a movable section, which are measured in real-time by two laser trackers on each side. As shown in Fig.3, both the

fixed section and the movable section are equipped with a docking reference hole at their docking end to establish their coordinate system. However, during the assembly process, the docking reference hole cannot be continuously measured due to the position interference caused by obstructions. Therefore, during the docking process, the coordinate system of the movable section is established by measuring the tracking ball located outside the movable section.

Before the assembly measurement begins, the position of the reference hole in relation to the tracking target ball must be determined and the transformation matrix established. There are four uniform positioning holes at the docking surface of the fixed section, which are called b_1, b_2, b_3, b_4, which can constitute the coordinate system of the fixed section O_B-$X_BY_BZ_B$. There are four positioning holes at the interface of the movable section, which are called h_1, h_2, h_3, h_4, and they can form the coordinate system of the movable section O_H-$X_HY_HZ_H$, and there are four tracking target balls outside the movable section for real-time monitoring during the docking process, which are called h_5, h_6, h_7, h_8, where b_1, b_2, b_3, b_4, h_1, h_2, h_3, h_4 are in a plane perpendicular to the geodetic reference system and $b_1b_3 \perp b_2b_4$, $h_1h_3 \perp h_2h_4$.
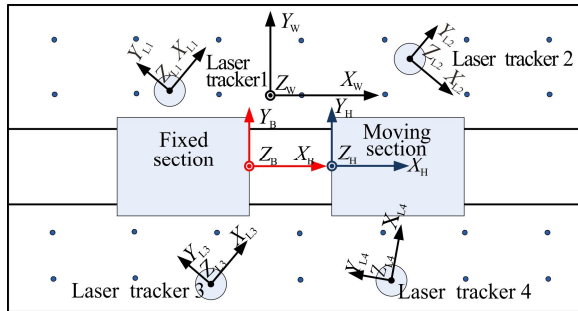

Fig.3 Position relationship of different coordinate systems

The global coordinate system, the laser tracker coor-

dinate system, the fixed section coordinate system, and the moving section coordinate system need to be established during the preparation phase.

First, establish the global coordinate system. The coordinates of the target point on the vertical beams A, B, C can be measured by laser rangefinder as

$$A:\left(X_{A_1}^L,Y_{A_1}^L,Z_{A_1}^L\right)^T,\left(X_{A_2}^L,Y_{A_2}^L,Z_{A_2}^L\right)^T \cdots\left(X_{A_n}^L,Y_{A_n}^L,Z_{A_n}^L\right)^T,$$

$$B:\left(X_{B_1}^L,Y_{B_1}^L,Z_{B_1}^L\right)^T,\left(X_{B_2}^L,Y_{B_2}^L,Z_{B_2}^L\right)^T \cdots\left(X_{B_n}^L,Y_{B_n}^L,Z_{B_n}^L\right)^T,$$

$$C:\left(X_{C_1}^L,Y_{C_1}^L,Z_{C_1}^L\right)^T,\left(X_{C_2}^L,Y_{C_2}^L,Z_{C_2}^L\right)^T \cdots\left(X_{C_n}^L,Y_{C_n}^L,Z_{C_n}^L\right)^T,(1)$$

where A, B, C denote the vertical beams in the plant, 1, 2, n are the numbers of different points and L denotes these are the coordinates in the laser tracker coordinate system.

The Z-axis of the global coordinate system is constructed by the point position on the vertical beam A. The vector line of the corresponding point position of AB is set as the direction of the X-axis of the global coordinate system, and the direction of the Y-axis of the global coordinate system is established by the right-hand rule.

Establish laser rangefinder coordinate system O_L-$X_LY_LZ_L$. The rotation angles around Z_L, Y_L, and X_L are defined as azimuth angle α, pitch angle β, and rolling angle γ, respectively.

$$\boldsymbol{R}_Z=\begin{bmatrix}\cos\alpha & -\sin\alpha & 0\\ \sin\alpha & \cos\alpha & 0\\ 0 & 0 & 1\end{bmatrix},$$

$$\boldsymbol{R}_Y=\begin{bmatrix}\cos\beta & 0 & \sin\beta\\ 0 & 1 & 0\\ -\sin\beta & 0 & \cos\beta\end{bmatrix},$$

$$\boldsymbol{R}_X=\begin{bmatrix}1 & 0 & 0\\ 0 & \cos\gamma & -\sin\gamma\\ 0 & \sin\gamma & \cos\gamma\end{bmatrix}. \qquad (2)$$

In this paper, the rotation order is first around the X_L-axis, then around the Y_L-axis, and finally around the Z_L-axis. Accordingly, the rotation matrix can be defined as

$$\boldsymbol{R} = \boldsymbol{R}_Z\boldsymbol{R}_Y\boldsymbol{R}_X =$$
$$\begin{bmatrix}\cos\alpha\cos\beta & \cos\alpha\sin\beta\sin\gamma-\sin\alpha\cos\gamma & \sin\alpha\sin\gamma+\cos\alpha\sin\beta\cos\gamma\\ \sin\alpha\cos\beta & \cos\alpha\cos\gamma+\sin\alpha\sin\beta\sin\gamma & \sin\alpha\sin\beta\cos\gamma-\cos\alpha\sin\gamma\\ -\sin\beta & \cos\beta\sin\gamma & \cos\beta\cos\gamma\end{bmatrix}=$$
$$\begin{bmatrix}b_{11} & b_{12} & b_{13}\\ b_{21} & b_{22} & b_{23}\\ b_{31} & b_{32} & b_{33}\end{bmatrix}. \qquad (3)$$

During the assembly process, the ranges of azimuth angle α, pitch angle β, and rolling angle γ will not exceed (−90°, +90°), that is, if the azimuth angle is within (−90°, +90°), since the value of $\cos\alpha$ can be determined as a positive value when both b_{33} and b_{11} are not zero, the expression is as follows

$$\alpha = \arctan(\frac{b_{32}}{b_{33}}),$$

$$\beta = -\arcsin(b_{31}),$$

$$\gamma = \arctan(\frac{b_{21}}{b_{11}}). \tag{4}$$

Establish the coordinate system of the fixed section O_B-$X_B Y_B Z_B$. The coordinates of the reference hole of the fixed section measured by the laser rangefinder are $P_{b1}^L, P_{b2}^L, P_{b3}^L, P_{b4}^L$. The average value of the coordinates of the reference hole measured by the laser rangefinder is written as $P_{bO}^L = [X_{bO}^L, Y_{bO}^L, Z_{bO}^L]$, and this coordinate is used as the origin of the coordinates in the laser rangefinder coordinate system. The radius at the end face of the fixed section is r, we can establish the fixed section coordinate system O_B-$X_B Y_B Z_B$ centered on the origin coordinate, the X_B-axis is perpendicular to the flange plane and points to the end of the movable part. The Z_B-axis is the $\overrightarrow{P_{bO} P_{b1}}$ direction, and the Y_B-axis is the $\overrightarrow{P_{bO} P_{b2}}$ direction. The moving section coordinate system O_H-$X_H Y_H Z_H$ is established in the same way as the fixed segment coordinate system.

After establishing all the above mentioned coordinate systems, we need to accurately calculate the conversion matrix between different coordinate systems for real-time pose control. In this paper, the least squares algorithm is used to calculate the conversion matrix.

Taking the coordinate system of the laser tracker to the global coordinate system as an example, the following formulas can be written according to the coordinate values of the global target in the laser rangefinder coordinate system and the global coordinate system.

$$\begin{bmatrix} X_{Gi}^W \\ Y_{Gi}^W \\ Z_{Gi}^W \end{bmatrix} = \begin{bmatrix} b_{11} & b_{12} & b_{13} \\ b_{21} & b_{22} & b_{23} \\ b_{31} & b_{32} & b_{33} \end{bmatrix} * \begin{bmatrix} X_{Gi}^L \\ Y_{Gi}^L \\ Z_{Gi}^L \end{bmatrix} + \begin{bmatrix} x \\ y \\ z \end{bmatrix}, \tag{5}$$

where $X_{Gi}^L (G=A, B, C; i=1, 2, 3 \cdots n)$ refers to the coordinate value of the global target on the vertical beam measured by the laser rangefinder, $X_{Gi}^W (G=A, B, C; i=1, 2, 3 \cdots n)$ represents the coordinate value assigned to the global target on the vertical beam in the global coordinate system, $b_{11}, b_{22} \ldots b_{33}, x, y, z$ are the parameters of the rotation matrix of the laser tracker coordinate system to the global coordinate system.

The relationship between all points can be expressed as Eq.(6) and Eq.(7), where $\overline{R_L^W}$ and $\overline{T_L^W}$ are the valuation in the rotation matrix and E_L^G is the estimated residuals of $\overline{P_{Gi}^W}$ and $\overline{R_L^W} P_{Gi}^L + \overline{T_L^W}$

$$P_{Gi}^W = \overline{R_L^W} P_{Gi}^L + \overline{T_L^W}, \tag{6}$$

$$E_L^G = \left(\overline{R_L^W} P_{Gi}^L + \overline{T_L^W} \right) - \overline{P_{Gi}^W}. \tag{7}$$

The least squares estimate requires the least sum of squares of the residuals[18]

$$J = \arg\min \sum_{i=1}^{3n} \left(E_L^G \right)^2 =$$

$$\arg\min \sum_{i=1}^{3n} \| (\overline{R_L^W} P_{Gi}^L + \overline{T_L^W}) - P_{Gi}^W \|^2. \tag{8}$$

The centroids corresponding to the points in the two sets of data sets are calculated respectively as Eq.(9) and Eq.(10), and use them to express the relationship between $\overline{R_L^W}$ and $\overline{T_L^W}$ as Eq.(11)

$$p_G^W = \frac{1}{3n} \sum_{i=1}^{3n} P_{Gi}^W, \tag{9}$$

$$p_G^L = \frac{1}{3n} \sum_{i=1}^{3n} P_{Gi}^L, \tag{10}$$

$$\overline{T_L^W} = p_G^W - \overline{R_L^W} p_G^L. \tag{11}$$

Substituting Eq.(11) into Eq.(8) for simplification, the error function can be simplified as

$$J = \arg\min \sum_{i=1}^{3n} \| \overline{R_L^W} P_{Gi}^{L'} - P_{Gi}^{W'} \|^2. \tag{12}$$

Multiple methods can be used to solve Eq.(12). In this paper, we chose to use singular value decomposition (SVD) to solve it. Compared to finding the minimum error at the extremes by direct derivation, SVD does not require matrix inversion, thus avoiding the problem of error amplification and achieving higher numerical stability. Moreover, using SVD avoids the situation where the result obtained through differentiation does not satisfy the orthogonal property.

The main steps are as follows.

Simplify Eq.(11) as follows, where $H = P_G^L \left(P_G^W \right)^T$,

$$J = \arg\min \sum_{i=1}^{3n} \| \overline{R_L^W} P_{Gi}^L - P_{Gi}^W \|^2 =$$

$$\arg\min \sum_{i=1}^{3n} \left(-2 \left(P_{Gi}^W \right)^T \overline{R_L^W} P_{Gi}^L \right) =$$

$$\arg\max \sum_{i=1}^{3n} \left(\left(P_{Gi}^W \right)^T \overline{R_L^W} P_{Gi}^L \right) =$$

$$\arg\max \left(\mathrm{trace} \left(\left(P_G^W \right)^T \overline{R_L^W} P_G^L \right) \right) =$$

$$\arg\max \left(\mathrm{trace}(\overline{R_L^W} H) \right). \tag{13}$$

We can decompose H by SVD as

$$H = U \Lambda V^T, \tag{14}$$

$$J = \arg\max \left(\mathrm{trace}(\overline{R_L^W} H) \right) \overset{H=U\Lambda V^T}{=}$$

$$\arg\max \left(\mathrm{trace}(\overline{R_L^W} U \Lambda V^T) \right) =$$

$$\arg\max \left(\mathrm{trace}(\Lambda V^T \overline{R_L^W} U) \right). \tag{15}$$

In order to take Eq.(14) to its maximum value, we can obtain the following relation, where I denotes the unit matrix, and thus find $\overline{R_L^W}$ and $\overline{T_L^W}$

$$I = V^T \overline{R_L^W} U, \tag{16}$$

$$\overline{R_L^W} = V U^T, \tag{17}$$

$$\overline{T_L^W} = p_G^W - \overline{R_L^W} p_G^L. \tag{18}$$

The same method can be used to find the optimal estimate from the fixed section coordinate system to the laser rangefinder coordinate system and from the moving section coordinate system to the laser rangefinder coordinate system.

After solving the above coordinate system conversion problem, we still need to solve the docking process position interference problem. The method we use is to use four laser rangefinders to measure the tracking target mirror on the outside of the moving section, and we can obtain its coordinates as $P_{h5}^{L}, P_{h6}^{L}, P_{h7}^{L}, P_{h8}^{L}$. Based on the r of the moving section coordinate system to the laser rangefinder coordinate system, the coordinates of the tracking target mirror on the outside of the moving section in the moving section coordinate system $P_{h5}^{H}, P_{h6}^{H}, P_{h7}^{H}, P_{h8}^{H}$ can be inferred, and the coordinates in the laser rangefinder coordinate can be used to determine the position of the moving section during the measurement.

To verify the effectiveness of the method proposed in this paper to realize the automatic docking of large-scale sections using multi-channel laser tracker real-time measurement, we set up a simulation docking experiment system for large-scale section docking. The experimental system adopts 4 sets of Leica AT901-LR laser trackers. Due to the restrictions of the indoor environment, we have made a reduced version of the large-scale docking section model. The diameter of the large-scale section produced is 1 125 mm, and the length is 800 mm. The four laser trackers are arranged on both sides of the large-scale section to be docked with 2 on each side. The distance between the laser tracker and the center axis of the large-scale section is 2 000 mm, and the distance between the laser trackers on the same side is 1 500 mm.

Fig.4 Experimental verification system for automatic docking of large sections

As shown in Fig.5, tracking target mirrors are installed on the measured section (moving section). Four laser trackers, which are the primary measuring equipment in the measurement system, are distributed across the two large-scale sections that need to be docked. These trackers will continuously measure the coordinate data of characteristic points on the mobile section by tracking the target mirror in real-time. The measurement system should be able to measure the 6-DOF position digitally and pose information of section products and have the functions of collecting, storing, and transmitting the six-degree-freedom position and pose data of section products to the control system simultaneously.

The software flow diagram of the measurement system is shown in Fig.6. The measurement system needs to confirm the global coordinate system, whether the coordinate system of the two docking segments is correctly established, and whether the four laser trackers correctly track the targets and establish a multi-station measurement system according to the actual layout of the section before the real-time measurement of the pose of the docking section. Once the measurement starts, the characteristic point data obtained by the four laser trackers will be collected by the measurement software in real time. The obtained coordinate data of the characteristic points will be substituted into the previous section pose calculation method with other known data in the measurement database to realize real-time continuous pose calculation of the measured sections. The final calculation result will be transmitted to the docking control system in real time.
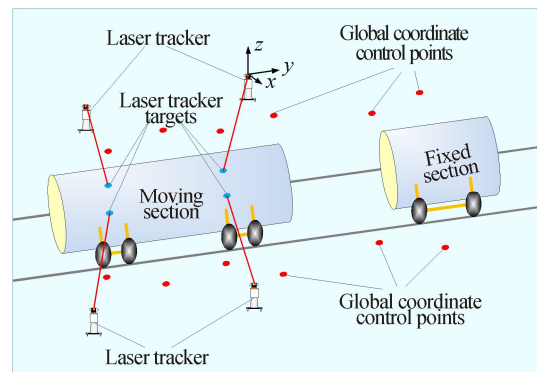

Fig.5 Measuring system diagram

In order to verify the accuracy of the joint station, we used a laser interferometer to set up several target points along the guideway direction in the docking section, and several sets of target points in the rotation direction according to the high-precision scale on the docking end face. We measured these points using the method described above and compared them with the actual positions to determine the displacement and rotation errors. The resulting data are shown in Tab.1. Through data analysis, we can see that in the pose measurement of the smaller large-scale section model considered in the experimental system, the actual error data is within half of the allowable error and has better accuracy redundancy.

Where the error of the target points along the guide rail is within 0.1 mm and the error in the direction of rotation is less than the specified 0.005 56°, which is in line with the actual requirements.
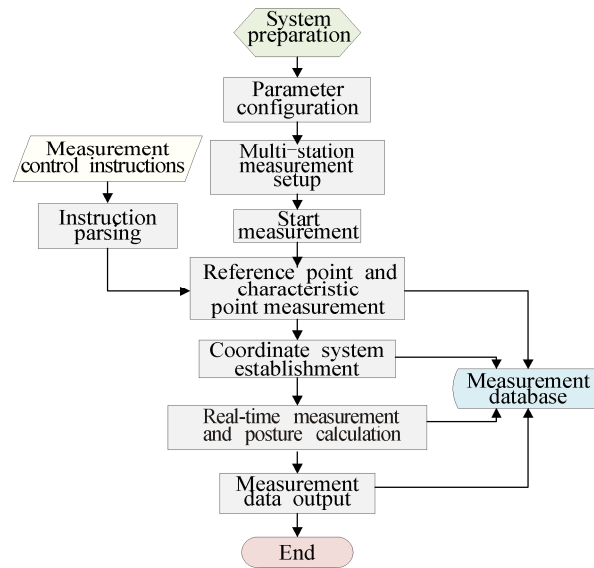

Fig.6 Flow chart of measurement system software

Tab.1 Error data for large-scale section model pose measurement

Measurement items	Measuring position	Measurement result		
		Maximum permissible error	δ_{max}	Evaluation
Displacement measurement error along the guide rail	$P_1\,(S_1=100\ mm)$	0.1	0.029 4	Qualified
	$P_2\,(S_2=200\ mm)$	0.1	0.023 4	Qualified
	$P_3\,(S_3=300\ mm)$	0.1	0.011 3	Qualified
	$P_4\,(S_4=400\ mm)$	0.1	0.019 7	Qualified
	$P_5\,(S_5=480\ mm)$	0.1	0.021 3	Qualified
Pose angle measurement error	$P_1\,(A_1=10°)$	0.005 556°	0.001 673°	Qualified
	$P_2\,(A_2=20°)$	0.005 556°	0.002 034°	Qualified
	$P_3\,(A_3=30°)$	0.005 556°	0.002 133°	Qualified
	$P_4\,(A_4=40°)$	0.005 556°	0.002 246°	Qualified
	$P_5\,(A_5=50°)$	0.005 556°	0.001 573°	Qualified
	$P_6\,(A_6=60°)$	0.005 556°	0.001 562°	Qualified
	$P_7\,(A_7=70°)$	0.005 556°	0.001 236°	Qualified
	$P_9\,(A_9=-10°)$	0.005 556°	0.000 426°	Qualified
	$P_{10}\,(A_{10}=-20°)$	0.005 556°	0.001 145°	Qualified
	$P_{11}\,(A_{11}=-30°)$	0.005 556°	0.001 736°	Qualified
	$P_{12}\,(A_{12}=-40°)$	0.005 556°	0.001 432°	Qualified
	$P_{13}\,(A_{13}=-50°)$	0.005 556°	0.000 693°	Qualified
	$P_{14}\,(A_{14}=-60°)$	0.005 556°	0.001 659°	Qualified
	$P_{15}\,(A_{15}=-70°)$	0.005 556°	0.001 457°	Qualified

In this paper, the feasibility of real-time measurement of docking sections and automatic docking was verified by 4-laser-traker combined measurement. In theory, measuring the pose of a rigid body requires tracking at least three points simultaneously. For more accurate measurement, the number of tracking points for large sections has been increased to improve the accuracy of measuring the pose of large-scale sections. The experimental system of this paper uses a reduced version of the rocket section model with a diameter of 1 125 mm. Although the measurement accuracy of this experimental system can perfectly meet the requirements of docking assembly accuracy, in the aerospace field, large sections can often reach diameters of 2 000 mm to 10 000 mm,

and their measurement and docking assembly accuracy still needs to be verified in practical applications.

Ethics declarations

Conflicts of interest

The authors declare no conflict of interest.

References

[1]   REN J, QUAN Q, LIU C, et al. Docking control for probe-drogue refueling：an additive-state-decomposition-based output feedback iterative learning control method[J]. Chinese journal of aeronautics, 2020, 33(3)：1016-1025.

[2]   WANG G, XIE Z J, MU X K, et al. Docking strategy for a space station container docking device based on adaptive sensing[J]. IEEE access, 2019, 7：100867-100880.

[3]   WANG M M, LI D S, ZHAO Y L. Iterative alignment of reflector panels for large-scale compact test range in non-metrology environment based on laser tracker[J]. Measurement science and technology, 2020, 31(4)：045002.

[4]   XUE Z, LIU J, WU C, et al. Review of in-space assembly technologies[J]. Chinese journal of aeronautics, 2020, 34(11)：21-47.

[5]   AHMAD N, BEHARA R, NARAYAN S S, et al. Simulation of spacecraft motion in separation test[J]. Journal of spacecraft technology, 2008, 18(2)：42-50.

[6]   JIANG J X, BIAN C, KE Y L. A new method for automatic shaft-hole assembly of aircraft components[J].Assembly automation, 2017, 37(1)：64-70.

[7]   LEI P, ZHENG L Y, XIAO W L, et al. A closed-loop machining system for assembly interfaces of large-scale component based on extended step-nc[J]. International journal of advanced manufacturing technology, 2017, 91(5-8)：2499-2525.

[8]   XU R, CHEN W, XU Y, et al. A new indoor positioning system architecture using gps signals[J]. Sensors, 2015, 15(5)：10074-10087.

[9]   ZHANG S F, LI B, REN F J, et al. High-precision measurement of binocular telecentric vision system with novel calibration and matching methods[J]. IEEE access, 2019, 7：54682-54692.

[10]   ZHANG X, XU Y Z, LI H C, et al. Flexible method for accurate calibration of large-scale vision metrology system based on virtual 3-D targets and laser tracker[J]. International journal of advanced robotic systems, 2019, 16(6)：172988141989351.

[11]   ZHA Q S, ZHU Y G, ZHANG W B. Visual and automatic wing-fuselage docking based on data fusion of heterogeneous measuring equipments[J]. Journal of the Chinese institute of engineers, 2021, 44(8)：792-802.

[12]   SUN C K, SUN P F, WANG P. An improvement of pose measurement method using global control points calibration[J]. Plos one, 2015, 10(7)：e0133905.

[13]   WANG T T, ZHANG Y M, LIU B. Model-based visual servoing for automatic docking system of circular symmetrical target with large displacement[J]. International journal of control automation and systems, 2023, 21(4)：1273-1284.

[14]   XI L, NI H S, WANG B Y, et al. Dynamic synthesis of three-point circle peripheral docking technology pose[J]. Applied sciences-basel, 2023, 13(4)：2685.

[15]   MURALIKRISHNAN B, PHILLIPS S, SAWYER D. Laser trackers for large-scale dimensional metrology：a review[J]. Precision engineering-journal of the international societies for precision engineering and nanotechnology, 2016, 44：13-28.

[16]   ROOS-HOEFGEEST S, GARCIA I A, GONZALEZ R C. Mobile robot localization in industrial environments using a ring of cameras and aruco markers[C]//IECON 2021-47th Annual Conference of the IEEE Industrial Electronics Society, October 13-16, 2021, Toronto, ON, Canada. New York：IEEE, 2021：21434270.

[17]   ZHANG H, JIANG C, LU M, et al. Design of robotic measuring system for large diameter pipe fittings based on line laser[C]//2022 14th International Conference on Measuring Technology and Mechatronics Automation (ICMTMA), January 15-16, 2022, Changsha, China. New York：IEEE, 2022：21666075.

[18]   CAO S M, CHENG Q L, GUO Y J, et al. Pose error compensation based on joint space division for 6-DOF robot manipulators[J]. Precision engineering-journal of the international societies for precision engineering and nanotechnology, 2022, 74：195-204.

[19]   GAO Y Z, GAO H B, BAI K P, et al. A robotic milling system based on 3D point cloud[J]. Machines, 2021, 9(12)：355.

[20]   ZHANG Y, CAI C G, LIU Z H, et al. Space-to-plane decoupling method for six-degree-of-freedom motion measurements[J]. Measurement science and technology, 2021, 32(12)：125005.